ACS APPLIED MATERIALS & INTERFACES

www.acsami.org

Research Article

On-Surface Synthesis of One-Dimensional Coordination Polymers with Tailored Magnetic Anisotropy

Benjamin Mallada, Piotr Błoński,* Rostislav Langer, Pavel Jelínek, Michal Otyepka, and Bruno de la Torre*

Cite This: *ACS Appl. Mater. Interfaces* 2021, 13, 32393−32401

Read Online

ACCESS | Metrics & More | Article Recommendations | Supporting Information

ABSTRACT: One-dimensional (1D) metalloporphyrin polymers can exhibit magnetism, depending on the central metal ion and the surrounding ligand field. The possibility of tailoring the magnetic signal in such nanostructures is highly desirable for potential spintronic devices. We present low-temperature (4.2 K) scanning tunneling microscopy and spectroscopy (LT-STM/STS) in combination with high-resolution atomic force microscopy (AFM) and a density functional theory (DFT) study of a two-step synthetic protocol to grow a robust Fe-porphyrin-based 1D polymer on-surface and to tune its magnetic properties. A thermally assisted Ullmann-like coupling reaction of Fe(III)diphenyl-bromine-porphyrin (2BrFeDPP-Cl) on Au(111) in ultra-high vacuum results in long (up to 50 nm) 1D metal−organic wires with regularly distributed magnetic and (electronically) independent porphyrins units, as confirmed by STM images. Thermally controlled C−H bond activation leads to conformational changes in the porphyrin units, which results in molecular planarization steered by 2D surface confinement, as confirmed by high-resolution AFM images. Spin-flip STS images in combination with DFT self-consistent spin−orbit coupling calculations of porphyrin units with different structural conformations reveal that the magnetic anisotropy of the triplet ground state of the central Fe ion units drops down substantially upon intramolecular rearrangements. These results point out to new opportunities for realizing and studying well-defined 1D organic magnets on surfaces and demonstrate the feasibility of tailoring their magnetic properties.

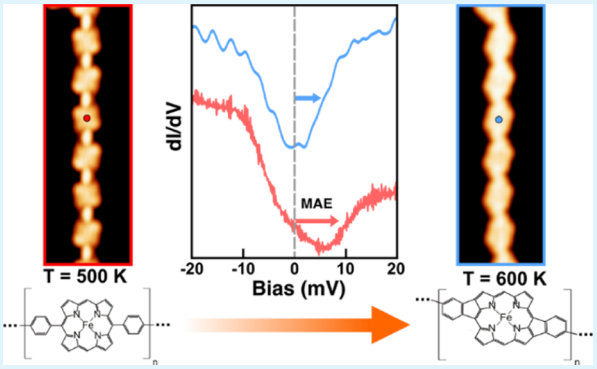

KEYWORDS: *coordination-polymer, on-surface chemistry, metal-porphyrin, magnetic anisotropy, scanning probe microscopy*

1. INTRODUCTION

The synthesis and functionalization of molecular spintronic nanostructures have attracted considerable interest due to their great potential for being beneficial to the next generation of electronic devices.[1−5] Among others, organic nanostructures enabling to tailor the spin-polarized signal is a burgeoning area of spintronic research.[5] One-dimensional (1D) polymeric organic magnets with regularly distributed magnetic centers are desirable networks, thanks to their long spin coherence length and mechanical flexibility.[6] Till date, several 1D molecular wires with transition-metal (TM) atoms have been proposed, including 1D TM-cyclopentadienyl,[7] TM-benzene,[8] TM-anthracene,[9] TM-phthalocyanine,[10] TM-metallocene,[11] TM-benzoquinonediimines,[12] and TM-naphthalene.[13] However, despite significant efforts, the experimental realization of such 1D polymeric molecular spintronics still remains a significant challenge. Nevertheless, the fabrication of novel frameworks that could be fashioned by a simple synthetic method is urgently required. To make progress in this field, it is important to choose a suitable functional molecule for making a large 1D polymeric framework.

Porphyrin molecules with coordinated TM atoms emerge as a promising candidate for constructing molecular spintronics because they combine inherent optical, redox, and magnetic properties of the intervening metal centers with those of the purely organic materials.[14−22] In such coordination polymer complexes, the ligand field coordinated with the central metal atom governs its magnetic anisotropy due to spin−orbit coupling (SOC).[23,24] Additionally, porphyrins exhibit high thermal stability and propensity to form well-ordered assemblies on a variety of solid surfaces.[25−27] Commonly, peripheral ligands are attached to the porphyrin macrocycle in specific positions in order to steer the intermolecular bonding.[28] Thus, arrays of conjugated porphyrin with delocalized electronic networks have been intensively explored

Received: March 12, 2021
Accepted: June 18, 2021
Published: July 6, 2021

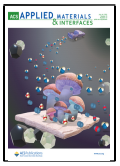

Chart 1. Thermal Reaction Sequence of 2BrFeDPP-Cl on Au(111) Obtained in the First Step of Annealing: Dehalogenation and Subsequent On-Surface Homocoupling Polymerization upon Annealing up to 500 K, and Furthermore, Cyclohydrogenation into cis- and trans-Polymers upon Annealing up to 600 K

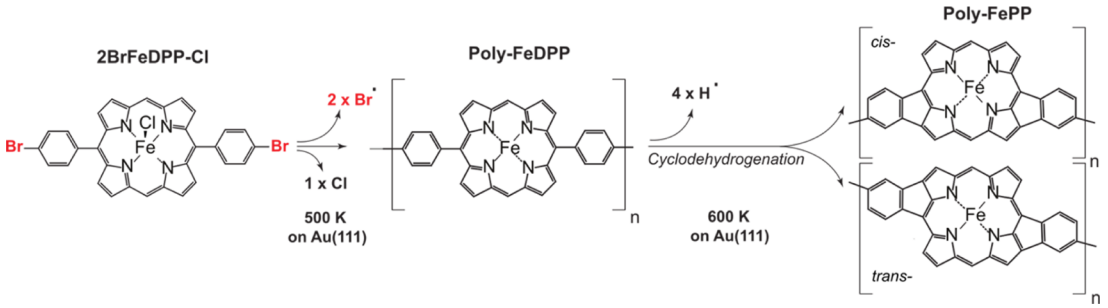

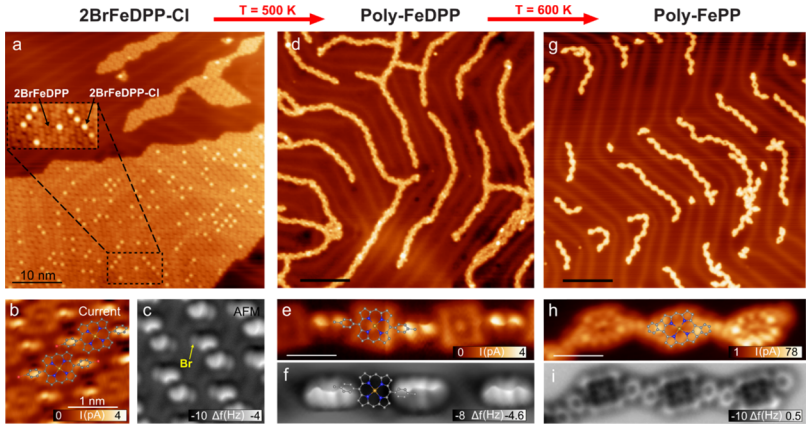

Figure 1. (a) STM topography upon deposition of 2BrFeDPP-Cl on Au(111) at RT (V_{bias} = −200 mV, I_{set} = 20 pA). (b,c) Detailed STM/nc-AFM constant height images with CO-tip. (d) STM topography upon sample annealing to 500 K (V_{bias} = 100 mV, I_{set} = 20 pA). (e,f) Corresponding detailed STM/nc-AFM constant height images with CO-tip of FeDPP molecular wires. (g) STM topography upon sample annealing to 600 K (V_{bias} = −500 mV, I_{set} = 50 pA). (h,i) Corresponding detailed STM/nc-AFM constant height images with CO-tip of the FePP molecular wires. The scale bar corresponds to 10 nm in (a,d,g) and to 1 nm in (b,c,e,f,h,i).

over the last two decades.[29−32] For example, the 1D Zn-porphyrin arrays have been already obtained experimentally, and they may find promising applications as a conducting molecule.[33]

However, such large structures are difficult to form by traditional chemical synthesis and to deposit on surfaces for further characterization and application onto devices; therefore, only oligomers formed by a few porphyrin units have been investigated so far. Recently, the emerging field of on-surface synthesis has enabled to overcome the limitation of both solubility and reactivity found in the solution synthesis, along with allowing in situ atomic-scale characterization by means of scanning tunneling microscopy/non-contact atomic force microscopy (STM/nc-AFM).[34] Furthermore, the 2D confinement imposed by the substrate during the polymerization process may result in molecular structure rearrangements, which would be otherwise difficult to induce as molecular planarization.

Here, we report a thorough investigation into the on-surface synthesis of large (up to 50 nm) metal-porphyrin based 1D molecular wires with regularly distributed magnetic and thermally adjustable anisotropy signals by means of low-temperature STM and high-resolution nc-AFM with CO-tip[35] complemented with theoretical calculations. Importantly, the formation of such long 1D chains have not been observed so far. Porphyrin building blocks are functionalized by bromine atoms in both phenyls at the para position, which steer an thermally induced intermolecular Ullman-like coupling reaction of aryl-halides, giving rise to 1D molecular wires, and further intramolecular transformations (planarization) at higher temperatures, allowing stepwise thermal control of chemical reactions.

We show that the adsorption of iron(III) 5,15-(di-4-bromophenyl)porphyrin-chloride molecules on Au(111) leads to the dechlorination of a large portion of molecules, which reduces the total spin of the molecule. Subsequent annealing to 500 K induces debromination, which gives rise to 1D molecular structures of covalently linked iron porphyrin molecules driven by aryl−aryl intermolecular coupling. A second step of annealing to 600 K affords intramolecular dehydrogenation and ring closure reactions as a consequence of activation at such a temperature of both C−H bonds of the aryl and porphyrin moieties, which results in molecular wires formed by iron-metaled planarized porphyrin molecules. Inelastic spin excitation experiments in combination with DFT calculations reveal a substantial modification of the magnetic anisotropy energy (MAE) at the iron atom upon porphyrin planarization due to the adjustment of the electron density at d and π orbitals.

We envision that our investigation into the magnetic anisotropy dependence and the spin−spin coupling in porphyrin-based molecular wires can provide insights into the magnetism, spin delocalization, metal−ligand d-π mixing,

https://doi.org/10.1021/acsami.1c04693
ACS Appl. Mater. Interfaces 2021, 13, 32393−32401

and pathways for transmitting spin effects in 1D molecular nanostructures.[36−40]

2. RESULTS

2.1. Structural Characterization. Chart 1 shows the chemical structure of the iron(III)-chlorine biphenyl porphyrin archetype [iron(III) 5,15-(di-4-bromophenyl)porphyrin chloride, hereafter referred to as 2BrFeDPP-Cl], we used as a molecular precursor in this study. This porphyrin species possesses phenyl moieties functionalized with C−Br groups at the para position to facilitate the linearity of the intermolecular coupling reaction product upon dehalogenation on the Au(111)substrate. Initial step-by-step structural characterization of the on-surface reaction was conducted by scanning probe microscopy (SPM) measurements to identify the distinct molecular structures present on the sample. Subsequently, after each sample annealing step, the sample is transferred and cooled to 5 K in ultra-high vacuum (UHV) conditions for SPM inspection.

2.1.1. Structure at 300 K. Upon adsorption at room temperature, 2BrFeDPP-Cl porphyrins were arranged into spatially extended close-packed islands with a majority of molecules appearing with a dim center, as depicted by STM images (cf. Figure 1). They correspond to the dechlorinated (loss of the Cl ligand) species 2BrFeDPP, which adopt a saddle conformation with twisted aryl moieties.[25,41] 2BrFeDPP molecules can be controllably realized by removing the Cl ligand from the 2BrFeDPP-Cl molecules using tunneling electrons over the Cl position[41] or by gently annealing the substrate (T < 500 K). The nc-AFM constant high images with CO-tip of assembled 2BrFeDPP molecules displayed a bonded Br atom as bright features (see Figure 1c), which correspond to strong repulsive force contributions, corroborating the preservation of bromine at the termini of both twisted phenyl moieties (cf. Figure 1b,c). According to the 2BrFeDPP optimized structure on Au(111) from DFT calculations (see Figure S1), the single molecule adsorbed preferentially on the Au(111) surface in a way that the Fe ion was directly above the Au atom of the top-most layer, with the adsorption energy of −77.4 kcal/mol at the Fe−Au distance of 3.53 Å. The in-plane rotation of the molecule, which decreased the Br−Br distance, increased the adsorption energy by at most 7.7 kcal/mol.

2.1.2. Structure at 500 K. A first step of the sample annealing to $T \sim 500$ K for 30 min led to the development of large 1D molecular wires extended over the surface (cf. Figure 1d). As illustrated by high-resolution STM/nc-AFM images, the molecular wires were composed of covalently bonded iron-porphyrin molecules that lost their coordinated chlorine atoms (cf. Figure 1e,f). Thus, we denote the subunits within the 1D structure as FeDPP, indicating the structural relationship with the precursor molecule. The annealing resulted in the cleavage of the C−Br bonds and the subsequent formation of 1D supramolecular structures upon surface-assisted aryl−aryl cross-coupling of adjacent porphyrin molecules. A wise choice of molecular functionalization in para positions at the porphyrin precursor allowed linearity during the intermolecular coupling process, which led to molecular wires with lengths that extend up to ∼40 monomers with no appreciable structural defects.

Importantly, the connecting aryl−aryl pairs were twisted owing to the steric hindrance, similar to unreacted 2BrFeTPP molecules on Au(111). Moieties at the same monomer were twisted differently; thus, consecutive bridges with opposite twist angle were observed within the 1D structures (cf. Figure 1e,f). In consequence, the non-planar configuration of the monomers hindered the submolecular resolution of the porphyrin centers by means of constant height nc-AFM imaging; therefore, only the linker moieties, which protruded further out of the surface, are featured in nc-AFM images (cf. Figures 1f and S2).

Finally, the loose end of the molecular wires was passivated by bromine or residual hydrogen atoms, precluding further polymerization. Interestingly, FeDPP molecular wires were easily manipulated with the SPM tip both vertically and laterally over the surface, which demonstrates the robustness of the nanostructure (see Figure S3).

2.1.3. Structure at 600 K. Following the thermal annealing of the molecule-decorated sample to $T \sim 600$ K for 30 min, molecular units within the wires underwent an intramolecular reaction through dehydrogenation and electrocyclic ring closure of their aryl termini and the macrocyclic pyrroles. This process led to the formation of isoindole motifs, which induced planarization of the porphyrin monomers on the surface (hereafter referred to as FePP units, Figure 1g), as unambiguously corroborated by high-resolution STM and nc-AFM images shown in Figure 1h,i. Therefore, the Fe atom at the center of the porphyrin unit is displayed as a cross-like feature in nc-AFM images, similar to the nc-AFM contrast observed on other metal phthalocyanines and porphyrin complexes.[42−44]

The ring closure of aryl moieties toward the macrocycle gave rise either to trans- or cis-configurations of the molecular repeating units (Chart 1). Statistically (over hundreds of monomer units counted on several samples), we observed equivalent abundance of the intramolecular cis (52%) and trans (48%) motifs, pointing out that both configurations are equally favorable. Interestingly, we found two effects regarding the substrate reconstruction: (1) the FePP molecular chains aligned along the herringbone, and, (2) frequently, the molecular chains terminated at the elbow sites. Thus, the segments that showed repeated cis or trans motifs were found with a maximum length of five units.

The intramolecular- versus intermolecular-induced reaction observed at different temperatures is rationalized by theoretical calculations of the dissociation energy (BDE) for various C−H and C−Br bonds of a single porphyrin specie on the Au(111) surface. Our theoretical calculations revealed that the activation energy for bromine abstraction was lower than that of hydrogen abstraction (C−H_1 and C−H_2, see bond labeling shown in Figure 2) by at least 30 kcal/mol (see Table 1). Upon adsorption, this value dropped up to 15 kcal/mol due to surface-assisted molecular structure stabilization. The initial removal of the Br atom further reduced the bond dissociation energies of the C−H_1, which favored H abstraction at higher temperatures, resulting in the ring closure of aryl moieties

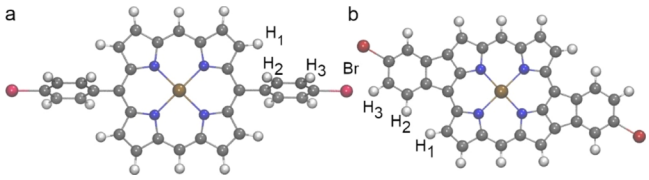

Figure 2. Stick-ball model for 2BrFeDPP (a) and 2BrFePP (b). BDEs of the labeled bonds are gathered in Table 1. C atoms are shown in gray, H in white, N in blue, Fe in orange, and Br in red.

https://doi.org/10.1021/acsami.1c04693
ACS Appl. Mater. Interfaces 2021, 13, 32393−32401

Table 1. BDEs (in kcal/mol) of C−Br and C−H Bonds Labeled in Figure 2a

	2BrFeDPP		2BrFePP	
bond	freestanding	on Au(111)	freestanding	on Au(111)
C−Br	99.3	102.1	85.3	102.8
$C-H_1$	133.2 (104.1)	117.9 (116.5)		118.5
$C-H_2$	129.5 (101.7)	128.2	128.1	117.8
$C-H_3$	129.8		116.2	115.8

[a]BDEs of selected C−H bonds after the removal of the Br atom are shown in brackets. See also note 1 in SOM on the calculated adsorption of 2BrFeDPP and 2BrFePP on Au(111).

steered by the 2D confinement of the surface. Thus, the stepwise annealing of 2BrFeDPP first allowed the formation of poly-FeDPP structures through Ullmann-like coupling of aryl-halides and, subsequently, the emergence of poly-FePP planar structures at higher temperatures. Interestingly, we found shorter molecular chains upon the planarization process (annealing at 600 K) in average (4−11 monomers). This may be due to thermally induced polymer breaking. However, molecular chains containing up to 50 nm can be found on the sample (see Figure S4).

Accordingly, annealing the sample at intermediate temperatures in the range of $T \sim 500-600$ K, that is, at 550 K, for 30 min, partially activated the ring closure reaction, thus yielding molecular wires with a mixture of FeDPP and FePP units (see Figure S5). Notably, no trace of intramolecular dehydrogenation was observed at temperatures below 550 K. Indeed, no dehydrogenation reaction was identified prior to the polymerization process of the molecular precursor.

On the other hand, annealing to elevated temperatures ($T >$ 600 K) resulted in molecular wires fused together, which reduced the 1D character of the nanostructures. These structures were formed by the dissociation of the C−H bonds at the periphery of the porphyrin units and by the subsequent fusion of the nearby polymer, as depicted in STM/nc-AFM images (see Figure S6).

2.2. Experimental Spin Features. Next, we focused on spin characteristics of 2BrFeDPP-Cl molecules upon adsorption, dechlorination, polymerization (poly-FeDPP), and intramolecular planarization (poly-FePP) by means of inelastic spin excitation spectroscopy with STM.[45−47] Figure 3 plots specific site spectra of the differential conductance (dI/dV) around the Fermi level with the STM tip placed on the Fe center (red) for both single 2BrFeDPP-Cl (Figure 3a) and 2BrFeDPP (Figure 3b) and on FeDPP (Figure 3c) and FePP (Figure 3d) units in a molecular wire as well. Reference spectroscopy on the bare Au(111) surface (featureless) is plotted with black lines, as shown in Figure 3.

In the case of 2BrFeDPP-Cl molecules, we identified a prominent dip feature at the Fermi level (cf. Figure 3a). In similar FeTPP-Cl molecules, step-like features at ±1.7 meV associated with spin-flip excitations have been reported.[48] However, due to the thermal broadening at the temperature at which we conducted our experiments (4.2 K), we cannot unequivocally distinguish weather the observed feature represents a spin-flip excitation or a Kondo resonance. The change in contrast between 2BrFeDPP-Cl and 2BrFeDPP (see Figure S7) is consistent with the same process in FeTPPCl (see, e.g., ref 41). In contrast, the spectra acquired on the Fe center of the dechlorinated 2BrFeDPP (cf. Figure 3b),

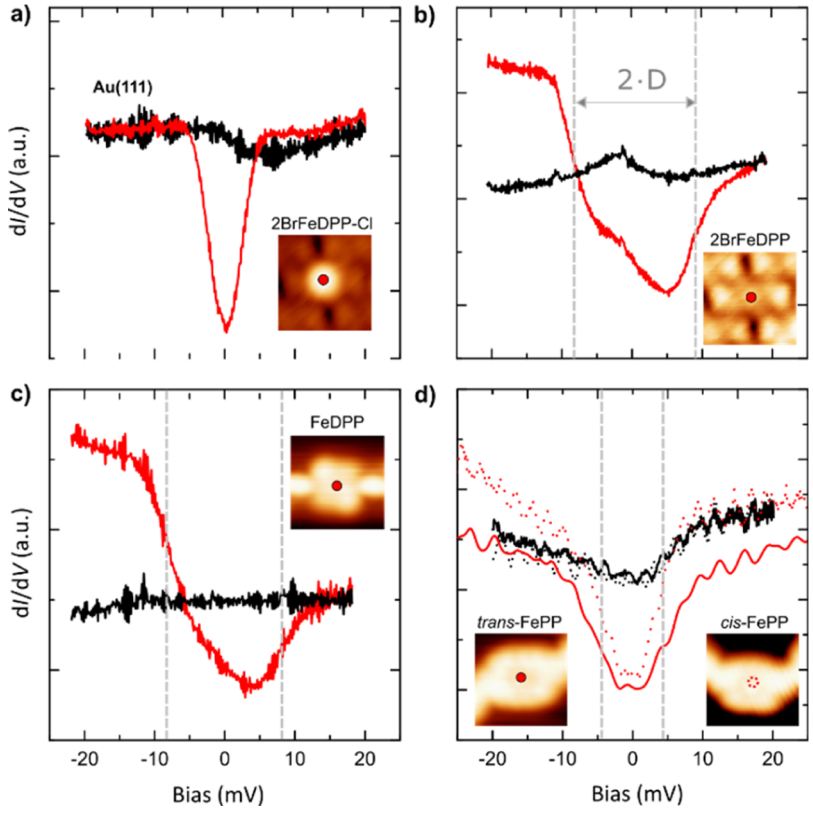

Figure 3. dI/dV spectra recorded on the center (red) of single 2BrFeDPP-Cl (a), on 2BrFeDPP (b), on monomer in poly-FeDPP wire, (c) on cis- (dash-shaped) and trans- (line-shaped) monomer in poly-FePP wire, and (d) corresponding reference spectra on the bare substrate (black).

https://doi.org/10.1021/acsami.1c04693
ACS Appl. Mater. Interfaces 2021, 13, 32393−32401

polymerized FeDPP (cf. Figure 3c), and FePP (cf. Figure 3d) molecules revealed stepwise increments in conductance at symmetric bias values. Consistent with previous studies on similar Fe-TPP on Au(111), we ascribed this feature to the spin-flip inelastic excitation process.[48,49]

Notably, the removal of the coordinated chlorine atom from the 2BrFeDPP-Cl molecules reduced the Fe-oxidation state from Fe^{3+} to Fe^{2+} and consequently lowered the total spin from S = 3/2 to S = 1.[41] The spin reduction was confirmed by the current SP-DFT calculations. Furthermore, the calculations predicted MAE of −4.1 meV for 2BrFeDPP-Cl, where the negative MAE represented the easy-axis system, which was in contrast with the MAE of dechlorinated 2BrFeDPP (cf. Section 3). Upon dechlorination, the degenerated triplet state splits into the ground spin state ms = 0 and the doubly degenerated ms = ±1 excited states due to the spin−orbit interaction. This splitting is referred to as zero-field splitting and occurs even in the absence of a magnetic field.[50] In the first approximation, the spin excitation is determined by the magnetic anisotropy of the molecule on the surface, which is well described by a spin Hamiltonian $HS_O = DS_z^2 + E(S_x^2 - S_y^2)$, where D is vertical magnetic anisotropy (origin of the zero-field splitting) and E is in-plane magnetic anisotropy, which typically vanishes for planar molecules. Therefore, we attributed the inelastic spin excitation spectra to the triplet S = 1, and the excitation energy corresponded to the axial anisotropy constant. It should be noted that very similar spectra were also obtained for an Fe-tetraphenyl-porphyrin molecule,[49] which was attributed to inelastic spin excitation of the S = 1 spin state as well.

The spectra acquired on the 2BrFeDPP molecules and FeDPP monomers showed excitation voltage onsets at V_s = ±8.5 mV and V_s = ±7.5 mV (see Figure S8), respectively (similar to previously reported values of D for FeDPP complexes[49]). It is worth noting that the difference in the excitation onset observed for 2BrFeDPP and FeDPP was lower than that in our experimental resolution (2 mV). Interestingly, the excitation spectra on both the 2BrFeDPP molecule and the FeDPP unit showed similar steps with asymmetric line shapes. Such asymmetries have been previously attributed to the characteristic particle-hole excitation symmetry in Fe-tetraphenyl porphyrin complexes.[48]

Based on this data and in accordance with our theoretical calculations (see below), we conclude that the polymerization process (aryl−aryl coupling) hardly affects the magnetic anisotropy of the FeDPP molecule (similar energy onset and line shape of the spin excitation). This result can be attributed to the lack of large distortions of the molecular ligand field upon the formation of poly-FeDPP chains, as confirmed by our calculations.

On the other hand, although the planarization process from poly-FeDPP toward poly-FePP did not change the overall character of the stepped spectrum (step-like shape), it decreased the onset of the excitation energy to V_s = ±3.5 mV (D = 3.5 meV). Additionally, the excitation in the FePP features had a more symmetric line shape than that in FeDPP. All together hint toward a change in the magnetic polarization of the spin state upon molecular planarization, as will be discussed below.

For comparison, we analyzed isolated FePP molecules, which were often found on the surface after annealing the sample to 600 K. They displayed identical characteristics to the corresponding FePP units in molecular wires (see Figure S9), confirming that the observed change in the MAE from FeDPP (D = 7.5 meV) to FePP (D = 3.5 meV) units was induced by planarization and the subsequent ligand field variation. Thus, we assume that the structure of the ligand field ruled the magnetic anisotropy of the wire units rather than that of the polymer bridges. This observation was further corroborated by measurements on a molecular chain composed of a mixture of FeDPP and FePP (see Figure S5), where we observed that the magnetic anisotropy of every molecular unit was not affected by being connected to either a planar or a non-planar unit. This result was expected due to the low degree of electronic delocalization of the single C−C bond connecting the monomers.

3. DISCUSSION

To gain a deeper insight into the origin of the reduction of MAE of the planarized FePP molecules observed experimentally, we performed spin-polarized DFT calculations including a self-consistent treatment of SOC. While the theoretical calculations of the MAE hinge on several inevitable approximations including the choice of an exchange−correlation functional, the degree of optimization of the geometry of the adsorbate/substrate complex, and the MAE calculated either self-consistently or via the magnetic force theorem, leading to a lower bound of the actual MAE, the theory still provides a sound physical picture of the MAE.[51] We examined the magnetic properties of the single molecules of 2BrFeDPP and 2BrFePP and polymers of FeDPP and FePP, both freestanding and supported on Au(111).

Scalar relativistic (SR) calculations predict the spin-triplet ground state for both the freestanding and Au(111)-supported molecules and chains, while the spin-singlet is at least ∼0.4 eV higher in energy. The total magnetic moment is localized mostly on the Fe ion and, to a much lesser extent, on the four coordinating N atoms (see Figure S10).

Table 2 gathers the theoretical MAE of all the systems considered. While the theoretical MAE of 2BrFeDPP and 2BrFePP is reduced by polymerization, the trend is reversed for the Au(111)-supported counterparts, due to the interaction with the substrate. The relative reduction of the MAE of the Au(111)-supported molecules and chains due to planarization is, however, similar and amounts to 1.7 and 2.0 meV, respectively. Thus, the reduction of MAE for the planarized molecules is in semi-quantitative agreement with the experimental observation, regardless of whether they were deposited on the Au(111) surface or/and polymerized. This indicates that the origin of the MAE reduction must be viewed in the differences in the symmetry of the Fe environment, which may lead to a different occupation scheme of the central Fe atom.

Table 2. MAE (in meV) of Freestanding and Au(111)-Supported 2BrFeDPP and 2BrFePP

	2BrFeDPP		2BrFePP	
	freestanding	on Au(111)	freestanding	on Au(111)
single molecule	6.2	2.0	1.0	0.3
dimer	4.8		1.1	
wire	1.5	3.7	0.4	1.7

[a]Positive MAE corresponds to an easy-plane system. The in-plane MAE of all systems was negligible.

https://doi.org/10.1021/acsami.1c04693
ACS Appl. Mater. Interfaces 2021, 13, 32393−32401

Indeed, in the 2BrFeDPP molecule, all Fe−N distances were equal to 2.01 Å. Occupations of the Fe 3d levels were similar for the SR limit and for the axial (hard) direction of magnetization after adding SOC (Figure S11). The rotation of magnetic moments in the in-plane (easy) direction led to the lifting of the degeneracy of the dπ states and the reordering and change in the occupation of the 3d levels.

In the 2BrFePP molecule, the square-planar symmetry was broken with two short and two long Fe−N bonds in the length of 1.94 and 2.04 Å, respectively, and the lifting of the degeneracy of the dπ states was already observed in the SR limit (see Figure S11). With SOC, no significant changes occurred in the occupation of the Fe 3d levels upon the rotation in the direction of magnetization between the axial (hard) and in-plane (easy) direction. This explains the reduced MAE in planarized 2BrFePP.

For a single molecule of 2BrFeDPP supported on Au(111), an in-plane magnetic direction is favored; as for a free-standing molecule (Table 2), with the spin/orbital moment of 2.361/0.113 μ_B. The perpendicular hard magnetic direction is disfavored by 2.0 meV with the spin/orbital moments reduced to 2.358/0.009 μ_B. The internal cyclization (planarization) reduced the MAE only to 0.3 meV, which is in line with the experimental observation. We identified the spin/orbital moments of 2.005/0.119 μ_B for the easy magnetic direction and 2.002/0.025 μ_B for the hard magnetic axis. It should be in line with the reduced anisotropy of the orbital moments, compared to the 2BrFeTPP/Au(111) system.

Densities of states of 2BrFeDPP/Au(111) and 2BrFePP/Au(111) projected on the Fe-d orbitals are shown in Figure 4a,b (see also Figures S12 and S13), and the corresponding occupation schemes of the Fe 3d levels are shown in Figure 4c,d. The $d_{x^2-y^2}$ and d_{xy}-derived states, which were localized and narrow due to their weak interaction with the Au substrate, were fully occupied and empty, respectively. While the spin-down d_{z^2} and dπ-derived states were occupied in both systems, for 2BrFeDPP/Au(111), the spin-up counterparts were partially occupied and empty, respectively. For planarized 2BrFePP/Au(111), the spin-up d_{z^2} and d_{xz}-derived states were both partially occupied, and, moreover, the d_{z^2} and dπ-derived states were slightly broadened because of their larger hybridization with the substrate. Accordingly, projected density of states (PDOS) indicates that the spin polarization originated predominantly from the contribution of d_{z^2} and dπ. As for the freestanding molecules, the degeneracy of dπ was largely broken for planarized 2BrFePP/Au(111) (Figures S12 and S13). In addition, the effect of SOC on the occupations of the 3d electronic states for the supported molecules was lower than that of the freestanding molecules (cf. Figure S11) as a consequence of the hybridization with the substrate and according to lower MAE[51] (cf. Table 2).

The occupation scheme of the 3d electronic states of the infinite chain of FeDPP and FePP supported on Au(111) corresponds well to those for the supported molecules (as shown in Figure 4c,d) and, accordingly, the MAE is in semi-qualitative agreement with the experimental findings. A slightly larger MAE, compared to the single-molecule counterparts, may be due to the intrachain interactions; this being at the expense of the interaction with the substrate.

4. CONCLUSIONS

In conclusion, we have synthesized large 1D metal-porphyrin wires on-surface and have investigated their conformational and intrinsic magnetic characteristics. High-resolution AFM images confirmed that annealing the 2BrFeDPP-Cl-decorated Au(111) sample to $T \approx 500$ K led to 1D polymers with regular Fe-porphyrins and surface-assisted intramolecular planarization upon sample annealing to $T \approx 600$ K. Such intramolecular planarization resulted in substantial adjustment of the magnetic properties of porphyrin's metal atom, as confirmed by spin-flip STS measurements and DFT-SOC calculations. Upon planarization, the MAE from the triplet ground state of the Fe ion dropped down due to a reduction of the ligand field symmetry and subsequent charge redistribution. We anticipate that the large flexibility of porphyrin compounds to incorporate different TM atoms and linkers into the macrocycle, together with the synthetic protocols presented here to control inter- and intramolecular on-surface reactions, may open new opportunities for designing π-d 1D nanostructures with desirable magnetic properties.

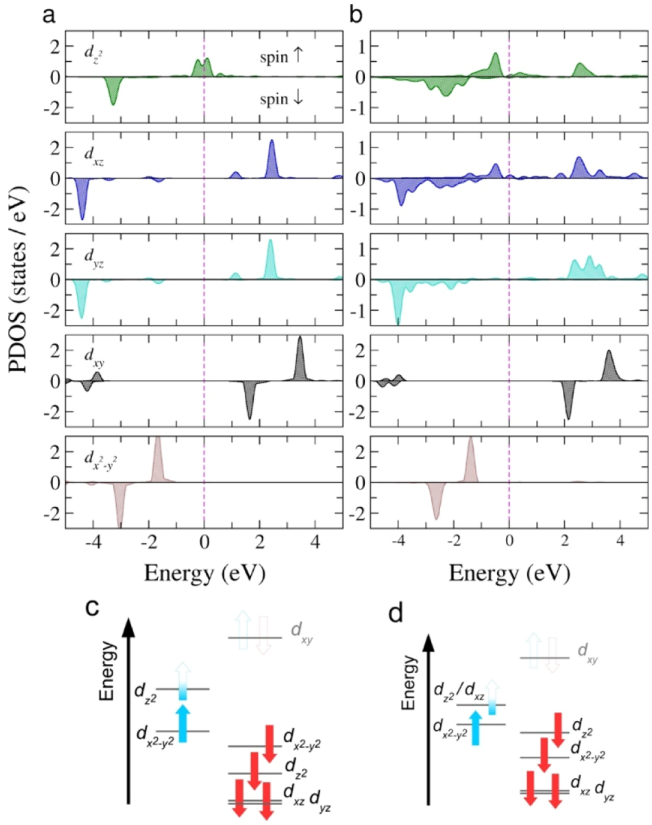

Figure 4. PDOS of the d orbitals of Fe for the Au(111)-supported 2BrFeDPP (a) and 2BrFePP (b). The corresponding PDOS-derived occupation schemes of Fe 3d levels are shown in (c,d). Due to two unpaired Fe-d electrons, the systems have S = 1 ground state (cf. Figures S12 and S13).

5. METHODS

5.1. Experimental Section. Experiments were performed in a custom-designed LT-STM/AFM UHV system (Createc GmbH) at 4.2 K with a base pressure below 5×10^{-10} mbar. STM/nc-AFM images were taken with sharpened focus ion beam Pt/Ir tips. STM images were acquired in the constant current mode with a bias voltage applied to the sample. For the spectroscopic measurements, specific site dI/dV were taken by a conventional lock-in technique with a modulation of 0.5 mV at 937 Hz. For nc-AFM imaging, the tip was functionalized with a single CO molecule picked up from the bare metal substrate and operated in the frequency-modulation mode

https://doi.org/10.1021/acsami.1c04693
ACS Appl. Mater. Interfaces 2021, 13, 32393−32401

(oscillated with a constant amplitude of 50 pm; resonant frequency ≈30 kHz; stiffness ≈1800 N/m). All nc-AFM images were acquired in a constant height mode with a bias voltage of 1 mV. All images were subject to a standard process using WSxM software.[52]

The Au(111) substrate was prepared by repeated cycles of Ar^+ sputtering (1 keV) and subsequent annealing. A molecular precursor (commercial from PorphyChem) was deposited by organic molecular-beam epitaxy from a tantalum pocket maintained at 625 K onto a clean Au(111) held at room temperature. When annealed to the desired temperature, the samples were transferred to the STM stage, which was maintained at 4.2 K.

5.2. Theoretical Calculations. DFT calculations[53,54] were performed with the Perdew−Burke−Ernzerhof exchange and correlation functional,[55] projected augmented wave potentials representing atomic cores,[56,57] and zero-damping DFT-D3 method of Grimme[58] to account for the dispersion corrections. The Hubbard $U - J = 4$ eV parameter[59] was applied for Fe. Occupations of the Fe 3d levels of freestanding molecules were re-examined by using non-local correlation functional optB86b + U.[60] The plane-wave basis set contained waves with kinetic energy lower than 500 eV. The Brillouin zone samplings were restricted to Γ point as the supercell dimensions were sufficiently large. Bond dissociation energies were computed by employing PBE0 hybrid functional[54,55,61] (see also Sen et al.[62]). The Au(111) surface was modeled using 7 × 7 supercells consisting of four Au layers, the bottom two layers of which were kept constrained in all structural relaxations. The vacuum layer of ∼15 Å was applied along the off-planar direction to ward off spurious interactions with the periodic images. Structural optimizations were performed employing a quasi-Newton algorithm until the residual atomic forces were below 25 meV $Å^{-1}$. Simultaneously, the electronic and magnetic degrees of freedom were converged to an energy of less than 10^{-6} eV. MAEs were computed in the noncollinear mode following implementations of Hobbs et al.[61] and Marsman and Hafner.[63] The adsorption energy E_{ad} of the BrFeDPP and 2BrFePP molecules on the Au(111) surface was calculated using the formula

$$E_{ad} = E_{tot} - E_{slab} - E_{molecule}$$

where E_{tot} represents the total energy of the entire surface-adsorbed system, E_{slab} is the total energy of the Au(111) slab, and $E_{molecule}$ is the total energy of the gas-phase 2BrFeDPP or 2BrFePP. In this convention, negative adsorption energy means that the adsorption is energetically favorable, and lower adsorption energy denotes higher energetic stability of the surface-adsorbed system.

■ ASSOCIATED CONTENT

Supporting Information

The Supporting Information is available free of charge at https://pubs.acs.org/doi/10.1021/acsami.1c04693.

Optimized structures of 2BrFeTPP [and 2BrFePP on Au(111)]; nc-AFM constant height images simulated using a DFT-calculated FeDPP dimer structure; lateral manipulation of FeDPP molecular chains; statistical distribution of chain lengths upon annealing the sample up to 600 K; overview after annealing the molecule decorated sample to 550 K; overview upon sample annealing to temperatures higher than 600 K; dechlorination of 2BrFeDPP-Cl molecule; measurements of the onset of magnetic anisotropy using the first derivative of the dI/dV spectra; characterization of single FePP molecule; isosurface of the spin density calculated for the 2BrFeDPP/Au(111) system; simplified scheme of the occupation of Fe 3d levels of the freestanding 2BrFeDPP and 2BrFePP; and spin- and orbital-resolved PDOS on Fe and N of 2BrFeDPP supported on Au(111) (PDF)

■ AUTHOR INFORMATION

Corresponding Authors

Piotr Błoński − *Regional Centre of Advanced Technologies and Material, Czech Advanced Technology and Research Institute (CATRIN), Palacký University Olomouc, 783 71 Olomouc, Czech Republic;* orcid.org/0000-0002-7072-232X; Email: piotr.blonski@upol.cz

Bruno de la Torre − *Regional Centre of Advanced Technologies and Material, Czech Advanced Technology and Research Institute (CATRIN), Palacký University Olomouc, 783 71 Olomouc, Czech Republic; Institute of Physics, The Czech Academy of Sciences, 162 00 Prague, Czech Republic;* orcid.org/0000-0002-6462-6833; Email: bdelatorre@fzu.cz

Authors

Benjamin Mallada − *Regional Centre of Advanced Technologies and Material, Czech Advanced Technology and Research Institute (CATRIN), Palacký University Olomouc, 783 71 Olomouc, Czech Republic; Institute of Physics, The Czech Academy of Sciences, 162 00 Prague, Czech Republic;* orcid.org/0000-0002-8209-9977

Rostislav Langer − *Regional Centre of Advanced Technologies and Material, Czech Advanced Technology and Research Institute (CATRIN), Palacký University Olomouc, 783 71 Olomouc, Czech Republic; Department of Physical Chemistry, Faculty of Science, Palacký University Olomouc, 78371 Olomouc, Czech Republic;* orcid.org/0000-0003-1703-6707

Pavel Jelínek − *Regional Centre of Advanced Technologies and Material, Czech Advanced Technology and Research Institute (CATRIN), Palacký University Olomouc, 783 71 Olomouc, Czech Republic; Institute of Physics, The Czech Academy of Sciences, 162 00 Prague, Czech Republic;* orcid.org/0000-0002-5645-8542

Michal Otyepka − *Regional Centre of Advanced Technologies and Material, Czech Advanced Technology and Research Institute (CATRIN), Palacký University Olomouc, 783 71 Olomouc, Czech Republic; IT4Innovations, Technical University of Ostrava, 708 00 Ostrava-Poruba, Czech Republic;* orcid.org/0000-0002-1066-5677

Complete contact information is available at: https://pubs.acs.org/10.1021/acsami.1c04693

Notes

The authors declare no competing financial interest.

■ ACKNOWLEDGMENTS

B.T. dedicates this work to the memory of José María Gómez-Rodriguez. The authors gratefully acknowledge support of the Operational Programme for Research, Development and Education of the European Regional Development Fund (project no. CZ.02.1.01/0.0/0.0/16_019/0000754). B.M. acknowledges support from the Internal Student Grant Agency of the Palacký University in Olomouc, Czech Republic (IGA_PrF_2021_032). R.L. acknowledges support from the Internal Student Grant Agency of the Palacký University in Olomouc, Czech Republic (IGA_PrF_2021_031). P.J. acknowledges support from the Praemium Academie of the Academy of Science of the Czech Republic and GACR (project no. 20-13692X).

REFERENCES

(1) Wolf, S. A. Spintronics: A Spin-Based Electronics Vision for the Future. *Science* **2001**, *294*, 1488−1495.
(2) Žutić, I.; Fabian, J.; Das Sarma, S. Spintronics: Fundamentals and Applications. *Rev. Mod. Phys.* **2004**, *76*, 323−410.
(3) Maslyuk, V. V.; Bagrets, A.; Meded, V.; Arnold, A.; Evers, F.; Brandbyge, M.; Bredow, T.; Mertig, I. Organometallic Benzene-Vanadium Wire: A One-Dimensional Half-Metallic Ferromagnet. *Phys. Rev. Lett.* **2006**, *97*, 097201.
(4) Wang, L.; Cai, Z.; Wang, J.; Lu, J.; Luo, G.; Lai, L.; Zhou, J.; Qin, R.; Gao, Z.; Yu, D.; Li, G.; Mei, W. N.; Sanvito, S. Novel One-Dimensional Organometallic Half Metals: Vanadium-Cyclopentadienyl, Vanadium-Cyclopentadienyl-Benzene, and Vanadium-Anthracene Wires. *Nano Lett.* **2008**, *8*, 3640−3644.
(5) Xiong, Z. H.; Wu, D.; Valy Vardeny, Z.; Shi, J. Giant Magnetoresistance in Organic Spin-Valves. *Nature* **2004**, *427*, 821−824.
(6) Tsukagoshi, K.; Alphenaar, B. W.; Ago, H. Coherent Transport of Electron Spin in a Ferromagnetically Contacted Carbon Nanotube. *Nature* **1999**, *401*, 572−574.
(7) Zhang, X.; Tian, Z.; Yang, S.-W.; Wang, J. Magnetic Manipulation and Half-Metal Prediction of One-Dimensional Bimetallic Organic Sandwich Molecular Wires [CpTM 1 CpTM 2] ∞ (TM 1 = Ti, Cr, Fe; TM 2 = Sc−Co). *J. Phys. Chem. C* **2011**, *115*, 2948−2953.
(8) Xiang, H.; Yang, J.; Hou, J. G.; Zhu, Q. One-Dimensional Transition Metal−Benzene Sandwich Polymers: Possible Ideal Conductors for Spin Transport. *J. Am. Chem. Soc.* **2006**, *128*, 2310−2314.
(9) Parida, P.; Kundu, A.; Pati, S. K. One-Dimensional Organometallic V−Anthracene Wire and Its B−N Analogue: Efficient Half-Metallic Spin Filters. *Phys. Chem. Chem. Phys.* **2010**, *12*, 6924.
(10) Ma, Y.; Dai, Y.; Zhang, Z.; Yu, L.; Huang, B. Magnetic Properties of Phthalocyanine-Based Organometallic Nanowire. *Appl. Phys. Lett.* **2012**, *101*, 062405.
(11) Santhini, V. M.; Stetsovych, O.; Ondráček, M.; Mendieta Moreno, J. I.; Mutombo, P.; Torre, B.; Švec, M.; Klívar, J.; Stará, I. G.; Vázquez, H.; Starý, I.; Jelínek, P. On-Surface Synthesis of Polyferrocenylene and its Single-Chain Conformational and Electrical Transport Properties. *Adv. Funct. Mater.* **2020**, *31*, 2006391.
(12) Santhini, V. M.; Wäckerlin, C.; Cahlík, A.; Ondráček, M.; Pascal, S.; Matěj, A.; Stetsovych, O.; Mutombo, P.; Lazar, P.; Siri, O.; Jelínek, P. 1D Coordination π−d Conjugated Polymers with Distinct Structures Defined by the Choice of the Transition Metal: Towards a New Class of Antiaromatic Macrocycles. *Angew. Chem., Int. Ed.* **2021**, *60*, 439−445.
(13) Telychko, M.; Su, J.; Gallardo, A.; Gu, Y.; Mendieta-Moreno, J. I.; Qi, D.; Tadich, A.; Song, S.; Lyu, P.; Qiu, Z.; Fang, H.; Koh, M. J.; Wu, J.; Jelínek, P.; Lu, J. Strain-Induced Isomerization in One-Dimensional Metal−Organic Chains. *Angew. Chem., Int. Ed.* **2019**, *58*, 18591−18597.
(14) Kang, B. K.; Aratani, N.; Lim, J. K.; Kim, D.; Osuka, A.; Yoo, K.-H. Length and Temperature Dependence of Electrical Conduction through Dithiolated Porphyrin Arrays. *Chem. Phys. Lett.* **2005**, *412*, 303.
(15) Tagami, K.; Tsukada, M.; Matsumoto, T.; Kawai, T. Electronic Transport Properties of Free-Base Tape-Porphyrin Molecular Wires Studied by Self-Consistent Tight-Binding Calculations. *Phys. Rev. B: Condens. Matter Mater. Phys.* **2003**, *67*, 245324.
(16) Long, M.-Q.; Chen, K.-Q.; Wang, L.; Qing, W.; Zou, B. S.; Shuai, Z. Negative Differential Resistance Behaviors in Porphyrin Molecular Junctions Modulated with Side Groups. *Appl. Phys. Lett.* **2008**, *92*, 243303.
(17) Ribeiro, F. J.; Lu, W.; Bernholc, J. Doping-Dependent Negative Differential Resistance in Hybrid Organic/Inorganic Si−Porphyrin−Si Junctions. *ACS Nano* **2008**, *2*, 1517−1522.
(18) Holten, D.; Bocian, D. F.; Lindsey, J. S. Probing Electronic Communication in Covalently Linked Multiporphyrin Arrays. A Guide to the Rational Design of Molecular Photonic Devices. *Acc. Chem. Res.* **2002**, *35*, 57−69.
(19) Yamaguchi, Y. Time-Dependent Density Functional Calculations of Fully π-Conjugated Zinc Oligoporphyrins. *J. Chem. Phys.* **2002**, *117*, 9688−9694.
(20) Chen, Y.; Prociuk, A.; Perrine, T.; Dunietz, B. D. Spin-Dependent Electronic Transport through a Porphyrin Ring Ligating an Fe(II) Atom: An Ab Initio Study. *Phys. Rev. B: Condens. Matter Mater. Phys.* **2006**, *74*, 245320.
(21) Abel, M.; Clair, S.; Ourdjini, O.; Mossoyan, M.; Porte, L. Single Layer of Polymeric Fe-Phthalocyanine: An Organometallic Sheet on Metal and Thin Insulating Film. *J. Am. Chem. Soc.* **2011**, *133*, 1203−1205.
(22) Zhou, J.; Sun, Q. Magnetism of Phthalocyanine-Based Organometallic Single Porous Sheet. *J. Am. Chem. Soc.* **2011**, *133*, 15113−15119.
(23) Carlin, R. L. Paramagnetism: Zero-Field Splittings. *Magnetochemistry*; Springer-Verlag: Berlin, 1986.
(24) Getzlaff, M. Magnetic Anisotropy Effects. *Fundamentals of Magnetism*; Springer-Verlag: Berlin, 2008.
(25) Auwärter, W.; Écija, D.; Klappenberger, F.; Barth, J. V. Porphyrins at Interfaces. *Nat. Chem.* **2015**, *7*, 105.
(26) Marbach, H. Surface-Mediated in Situ Metalation of Porphyrins at the Solid−Vacuum Interface. *Acc. Chem. Res.* **2015**, *48*, 2649−2658.
(27) Gottfried, J. M. Surface Chemistry of Porphyrins and Phthalocyanines. *Surf. Sci. Rep.* **2015**, *70*, 259−379.
(28) Jurow, M.; Schuckman, A. E.; Batteas, J. D.; Drain, C. M. Porphyrins as Molecular Electronic Components of Functional Devices. *Coord. Chem. Rev.* **2010**, *254*, 2297−2310.
(29) Tanaka, T.; Osuka, A. Conjugated Porphyrin Arrays: Synthesis, Properties and Applications for Functional Materials. *Chem. Soc. Rev.* **2015**, *44*, 943−969.
(30) Judd, C. J.; Nizovtsev, A. S.; Plougmann, R.; Kondratuk, D. V.; Anderson, H. L.; Besley, E.; Saywell, A. Molecular Quantum Rings Formed from a π -Conjugated Macrocycle. *Phys. Rev. Lett.* **2020**, *125*, 206803.
(31) Svatek, S. A.; Perdigão, L. M. A.; Stannard, A.; Wieland, M. B.; Kondratuk, D. V.; Anderson, H. L.; O'Shea, J. N.; Beton, P. H. Mechanical Stiffening of Porphyrin Nanorings through Supramolecular Columnar Stacking. *Nano Lett.* **2013**, *13*, 3391−3395.
(32) Saywell, A.; Browning, A. S.; Rahe, P.; Anderson, H. L.; Beton, P. H. Organisation and Ordering of 1D Porphyrin Polymers Synthesised by On-Surface Glaser Coupling. *Chem. Commun.* **2016**, *52*, 10342−10345.
(33) Tsuda, A. Fully Conjugated Porphyrin Tapes with Electronic Absorption Bands That Reach into Infrared. *Science* **2001**, *293*, 79−82.
(34) Grill, L.; Hecht, S. Covalent On-Surface Polymerization. *Nat. Chem.* **2020**, *12*, 115−130.
(35) Jelínek, P. High Resolution SPM Imaging of Organic Molecules with Functionalized Tips. *J. Phys.: Condens. Matter* **2017**, *29*, 343002.
(36) Iwamura, H.; Koga, N. Studies of Organic Di-, Oligo-, and Polyradicals by Means of Their Bulk Magnetic Properties. *Acc. Chem. Res.* **1993**, *26*, 346−351.
(37) Ung, V. Â.; Cargill Thompson, A. M. W.; Bardwell, D. A.; Gatteschi, D.; Jeffery, J. C.; McCleverty, J. A.; Totti, F.; Ward, M. D. Roles of Bridging Ligand Topology and Conformation in Controlling Exchange Interactions between Paramagnetic Molybdenum Fragments in Dinuclear and Trinuclear Complexes. *Inorg. Chem.* **1997**, *36*, 3447−3454.
(38) Pardo, E.; Carrasco, R.; Ruiz-García, R.; Julve, M.; Lloret, F.; Muñoz, M. C.; Journaux, Y.; Ruiz, E.; Cano, J. Structure and Magnetism of Dinuclear Copper(II) Metallacyclophanes with Oligoacenebis(Oxamate) Bridging Ligands: Theoretical Predictions on Wirelike Magnetic Coupling. *J. Am. Chem. Soc.* **2008**, *130*, 576−585.
(39) Ferrando-Soria, J.; Castellano, M.; Yuste, C.; Lloret, F.; Julve, M.; Fabelo, O.; Ruiz-Pérez, C.; Stiriba, S.-E.; Ruiz-García, R.; Cano, J. Long-Distance Magnetic Coupling in Dinuclear Copper(II) Com-

https://doi.org/10.1021/acsami.1c04693
ACS Appl. Mater. Interfaces 2021, 13, 32393−32401

plexes with Oligo-Para-Phenylenediamine Bridging Ligands. *Inorg. Chim. Acta* **2010**, *363*, 1666−1678.
(40) Castellano, M.; Fortea-Pérez, F. R.; Stiriba, S.-E.; Julve, M.; Lloret, F.; Armentano, D.; De Munno, G.; Ruiz-Garcı, R.; Cano, J. Very Long-Distance Magnetic Coupling in a Dicopper(II) Metallacyclophane with Extended π-Conjugated Diphenylethyne Bridges. *Inorg. Chem.* **2011**, *50*, 11279−11281.
(41) Gopakumar, T. G.; Tang, H.; Morillo, J.; Berndt, R. Transfer of Cl Ligands between Adsorbed Iron Tetraphenylporphyrin Molecules. *J. Am. Chem. Soc.* **2012**, *134*, 11844.
(42) Kaiser, K.; Gross, L.; Schulz, F. A Single-Molecule Chemical Reaction Studied by High-Resolution Atomic Force Microscopy and Scanning Tunneling Microscopy Induced Light Emission. *ACS Nano* **2019**, *13*, 6947−6954.
(43) Chutora, T.; de la Torre, B.; Mutombo, P.; Hellerstedt, J.; Kopeček, J.; Jelínek, P.; Švec, M. Nitrous Oxide as an Effective AFM Tip Functionalization: A Comparative Study. *Beilstein J. Nanotechnol.* **2019**, *10*, 315−321.
(44) Doležal, J.; Merino, P.; Redondo, J.; Ondič, L.; Cahlík, A.; Švec, M. Charge Carrier Injection Electroluminescence with CO-Functionalized Tips on Single Molecular Emitters. *Nano Lett.* **2019**, *19*, 8605−8611.
(45) Heinrich, A. J.; Gupta, J. A.; Lutz, C. P.; Eigler, D. M. Single-Atom Spin-Flip Spectroscopy. *Science* **2004**, *306*, 466.
(46) Madhavan, V. Tunneling into a Single Magnetic Atom: Spectroscopic Evidence of the Kondo Resonance. *Science* **1998**, *280*, 567−569.
(47) Ternes, M. Spin Excitations and Correlations in Scanning Tunneling Spectroscopy. *New J. Phys.* **2015**, *17*, 063016.
(48) Rubio-Verdú, C.; Sarasola, A.; Choi, D.-J.; Majzik, Z.; Ebeling, R.; Calvo, M. R.; Ugeda, M. M.; Garcia-Lekue, A.; Sánchez-Portal, D.; Pascual, J. I. Orbital-Selective Spin Excitation of a Magnetic Porphyrin. *Commun. Phys.* **2018**, *1*, 15.
(49) Li, J.; Merino-Díez, N.; Carbonell-Sanromà, E.; Vilas-Varela, M.; De Oteyza, D. G.; Peña, D.; Corso, M.; Pascual, J. I. Survival of Spin State in Magnetic Porphyrins Contacted by Graphene Nanoribbons. *Sci. Adv.* **2018**, *4*, No. eaaq0582.
(50) Tsukahara, N.; Noto, K.-i.; Ohara, M.; Shiraki, S.; Takagi, N.; Takata, Y.; Miyawaki, J.; Taguchi, M.; Chainani, A.; Shin, S.; Kawai, M. Adsorption-Induced Switching of Magnetic Anisotropy in a Single Iron(II) Phthalocyanine Molecule on an Oxidized Cu(110) Surface. *Phys. Rev. Lett.* **2009**, *102*, 167203.
(51) Błoński, P.; Hafner, J. Density-Functional Theory of the Magnetic Anisotropy of Nanostructures: An Assessment of Different Approximations. *J. Phys.: Condens. Matter* **2009**, *21*, 426001.
(52) Horcas, I.; Fernández, R.; Gómez-Rodríguez, J. M.; Colchero, J.; Gómez-Herrero, J.; Baro, A. M. WSXM: A Software for Scanning Probe Microscopy and a Tool for Nanotechnology. *Rev. Sci. Instrum.* **2007**, *78*, 013705.
(53) Kresse, G.; Hafner, J. Ab Initio Molecular Dynamics for Liquid Metals. *Phys. Rev. B: Condens. Matter Mater. Phys.* **1993**, *47*, 558−561.
(54) Kresse, G.; Furthmüller, J. Efficiency of Ab-Initio Total Energy Calculations for Metals and Semiconductors Using a Plane-Wave Basis Set. *Comput. Mater. Sci.* **1996**, *6*, 15−50.
(55) Perdew, J. P.; Burke, K.; Ernzerhof, M. Generalized Gradient Approximation Made Simple. *Phys. Rev. Lett.* **1996**, *77*, 3865−3868.
(56) Blöchl, P. E. Projector Augmented-Wave Method. *Phys. Rev. B: Condens. Matter Mater. Phys.* **1994**, *50*, 17953.
(57) Kresse, G.; Joubert, D. From Ultrasoft Pseudopotentials to the Projector Augmented-Wave Method. *Phys. Rev. B: Condens. Matter Mater. Phys.* **1999**, *59*, 1758−1775.
(58) Grimme, S.; Antony, J.; Ehrlich, S.; Krieg, H. A Consistent and Accurate Ab Initio Parametrization of Density Functional Dispersion Correction (DFT-D) for the 94 Elements H-Pu. *J. Chem. Phys.* **2010**, *132*, 154104.
(59) Dudarev, S. L.; Botton, G. A.; Savrasov, S. Y.; Humphreys, C. J.; Sutton, A. P. Electron-Energy-Loss Spectra and the Structural Stability of Nickel Oxide: An LSDA+U Study. *Phys. Rev. B: Condens. Matter Mater. Phys.* **1998**, *57*, 1505−1509.
(60) Klimeš, J.; Bowler, D. R.; Michaelides, A. Van Der Waals Density Functionals Applied to Solids. *Phys. Rev. B: Condens. Matter Mater. Phys.* **2011**, *83*, 195131.
(61) Hobbs, D.; Kresse, G.; Hafner, J. Fully Unconstrained Noncollinear Magnetism within the Projector Augmented-Wave Method. *Phys. Rev. B: Condens. Matter Mater. Phys.* **2000**, *62*, 11556−11570.
(62) Sen, D.; Błoński, P.; Torre, B. d. l.; Jelínek, P.; Otyepka, M. Thermally Induced Intra-Molecular Transformation and Metalation of Free-Base Porphyrin on Au(111) Surface Steered by Surface Confinement and Ad-Atoms. *Nanoscale Adv.* **2020**, *2*, 2986.
(63) Marsman, M.; Hafner, J. Broken Symmetries in the Crystalline and Magnetic Structures of γ-Iron. *Phys. Rev. B: Condens. Matter Mater. Phys.* **2002**, *66*, 224409.

https://doi.org/10.1021/acsami.1c04693
ACS Appl. Mater. Interfaces 2021, 13, 32393−32401